Surfaces and Interfaces 38 (2023) 102830

Contents lists available at ScienceDirect

Surfaces and Interfaces

journal homepage: www.sciencedirect.com/journal/surfaces-and-interfaces

A facile preparation method for efficiency a novel $LaNiO_3/SrCeO_3$ (p-n type) heterojunction catalyst in photocatalytic activities, bactericidal assessment and dopamine detection

Ying Chen [a], Ali Jihad [b], Fadhil Hussam [c], Salah Hassan Zain Al-Abdeen [d], Jamal Mohammad Hussein [e], Zainab Hussein Adhab [f], Zahraa Hamzaa Abd Alzahraa [g], Irfan Ahmad [h], Leila Fatolahi [i], Baadal Jushi Janani [j,*]

[a] Chongqing Academy of Governance, Jiulongpo district, Chongqing 400039, China
[b] Department of Pharmacy, Al- Mustaqbal University College, Babylon 51001, Iraq
[c] College of Medical Technology, Medical Lab techniques, Al-Farahidi University, Iraq
[d] Department of Medical Laboratories Technology, Al-Nisour University College, Baghdad, Iraq
[e] Department of Medical Laboratory Technics, AlNoor University College, Nineveh, Iraq
[f] Department of Pharmacy, Al-Zahrawi University College, Karbala, Iraq
[g] National University of Science and Technology, Dhi Qar, Iraq
[h] Department of Clinical Laboratory Sciences, College of Applied Medical Sciences, King Khalid University, Abha, Saudi Arabia
[i] Department of Chemistry, Payame Noor University, Tehran, Iran
[j] Department of Chemistry, Academy of Materials Science, Navi Mumbai, India

ARTICLE INFO

Keywords:
Nanocomposite
p-n type heterojunction
Photocatalytic
Bactericidal
Colorimetric

ABSTRACT

The wide occurrence of medicines and textiles pollutants in water bodies, as well as their by-products, has raised concerns about the impact of damage to the environment and human health. In this study, the photocatalytic effect of Lanthanum nickelate ($LaNiO_3$), strontium cerate ($SrCeO_3$), and $LaNiO_3/SrCeO_3$ nanocomposite were studied using the co-precipitation method at room temperature. Various techniques were used to analyze the structural, morphological, optical properties of these synthesized nanoparticles. The results indicates uniform growth of $LaNiO_3$ nanoparticles on the surface of $SrCeO_3$ nanoparticles in sphere-shaped forms which confirms the formation of a p-n type junction catalyst. The energy bandgap of $SrCeO_3$, $LaNiO_3$ and $LaNiO_3/SrCeO_3$ was found to be 2.79, 2.06, and 1.65 eV, respectively. The photocatalytic activity was studied by degradation of Methylene Blue dye under visible light. As a result, reusability test shows the stability of catalysts for long-term period. The $LaNiO_3/SrCeO_3$ composites depicts the effective degradation for MB dye was 93.5% at 100 min. The rate constant (K, min^{-1}) of $SrCeO_3$, $LaNiO_3$, and $LaNiO_3/SrCeO_3$ was 0.0050, 0.0088, and 0.0156, respectively. The antibacterial action of $LaNiO_3/SrCeO_3$ versus *Klebsiella pneumoniae* and *Bacillus cereus* observed by using the antimicrobial test. The peroxidase activity of $LaNiO_3/SrCeO_3$ was performed for colorimetric detection of dopamine. The linear range of the method is 1-200 nM via the detection limit of 3.48 μM. The $LaNiO_3/SrCeO_3$ has high potential in analysis of dopamine.

1. Introduction

Water pollution has arisen as a key concern for the scientific community in recent years, with fast-rising businesses and populations, necessitating an intensive and valid response. Colored dyes used in the textile industry, like methylene blue are harmful to aquatic life and people who suffer from skin diseases, and lung infections [1–3]. As a result, a novel low-cost way of eliminating these dyes before releasing them into the environment is required [4]. There are several ways to decompose these organic pollutants in wastewater, but advanced oxidation processes are still a fairly new technique [5–7]. The best methods for reducing pollutants in wastewater systems is photocatalytic degradation with semiconductor photocatalysts [8–11]. Previous research has shown that heterogeneous photocatalysts are particularly

* Corresponding author at: Department of Chemistry, Academy of Materials Science, Navi Mumbai, India
E-mail address: bajujanani@gmail.com (B.J. Janani).

https://doi.org/10.1016/j.surfin.2023.102830
Received 24 December 2022; Received in revised form 6 March 2023; Accepted 21 March 2023
Available online 22 March 2023

effective in removing a wide impurities from our wastewater system [12–16]. Various metal oxides, such as TiO_2, Fe_2O_3, ZnO, ZrO_2, Nb_2O_5, V_2O_5, and WO_3, have been employed as excellent catalysts for photocatalytic water treatment [17–20]. Hybrid semiconductor materials produced by p-n-type heterostructures are an extremely effective way of removing organic contaminants [21]. Hybrid semiconductor materials such as TiO_2-SnO_2 [22], CuO-ZnO [23], Mn_2CuO_4/CdO [14], $SnFe_2O_4$/$BiFeO_3$ [24] are widely used for photocatalysis process. The use of rare earth metal oxide such as Lanthanum nickelate ($LaNiO_3$), and strontium cerate ($SrCeO_3$) with band gaps at ~2.0 eV and 3.0 eV, is the new technique in photocatalysis system [25–27]. These minerals are used frequently to enhance chemical resistance, luminescence, and mechanical strength and have exciting applications in the industrial and technological fields [25]. Because of its crystal structure, and high oxygen storage capacity, $SrCeO_3$ has received a lot of interest in the photocatalytic degradation of wastewater pollutants [27]. Because the activities and selection of pure $SrCeO_3$ catalysts are generally increased by modifying the morphology and particle size. The catalytic oxidation can be modified by the $LaNiO_3$ [26]. The $LaNiO_3$, which has remarkable properties and is a prospective material in many industries [26].

The important hormone in human body is dopamine (DA). The presence of DA is necessary to maintain the normal activity of the body. Abnormal amount of DA will bad effect on human health and nervous system diseases, such as schizophrenia, and Parkinson's disease were conducted [28]. Thereupon, the quantitative DA detection method is essential for disease diagnosis. The colorimetric technique has many benefits such as facile operation and low cost, and this great for detection of DA [14].

In this study, the synthesize $LaNiO_3$/$SrCeO_3$ heterostructures was conducted by a precipitation technique. The physiochemical, optical, and structural aspects of $LaNiO_3$/$SrCeO_3$ nanostructures were investigated and the photocatalytic degradation capacity was conducted by employing the MB as a pollutant. The reusability analysis of the $LaNiO_3$/$SrCeO_3$ nanocomposites was conducted to investigate the stability of catalysts for usage. The antibacterial properties of the $LaNiO_3$/$SrCeO_3$ was conducted against *Klebsiella pneumoniae* and *Bacillus cereus.* The peroxidase like activity of the $LaNiO_3$/$SrCeO_3$ nanocomposites was studied in the colorimetric detection of DA. The detection limit was calculated.

2. Experimental

2.1. Chemicals

Materials and reagents are provided in Support Information Text S1.

2.2. Fabrication of $LaNiO_3$/$SrCeO_3$ Nanocomposites

Nanocomposite (p-type $LaNiO_3$/n-type $SrCeO_3$) catalysts were fabricated by using the co-precipitation method in two steps. In first solution, 0.3 M of lanthanum nitrate hexahydrate, 0.3 M of Nickel nitrate hexahydrate and 0.5 M of sodium hydroxide was dissolved in 150 mL distilled water, which was stirred with a magnetic stirrer for about 50°C for 3 hours. Similarly, in second solution, 0.3 M of cerium nitrate hexahydrate and 0.3 M of strontium nitrate were dissolving in 150 mL distilled water, which was stirred with a magnetic stirrer for about 50°C for 3 hours and 0.5 M of sodium hydroxide solution was added drop by drop until the pH of the solution rises to pH-10. The precipitate was washed and dried at 90°C for 8 h.

To make a suspension, the $LaNiO_3$ and $SrCeO_3$ samples were mixed with ethanol as a liquid solvent. The $LaNiO_3$ powder was dispersed in 100 ml ethanol for 2 hours using a magnetic stirrer. Then, in a similar ratio of (1:1) $SrCeO_3$ powder was added to the suspension and mixed until a homogeneous mixture was formed. After evaporate the solvent, the product was aged at 150°C for 6 h, and calcined at 500°C for 3 h.

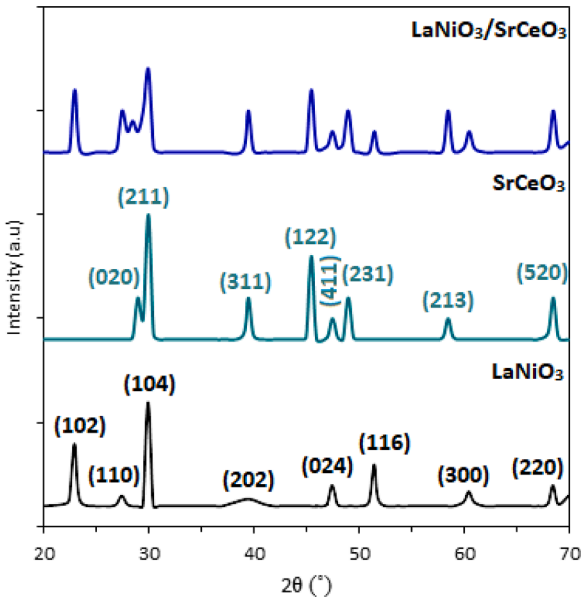

Fig. 1. XRD Patterns of synthesis $LaNiO_3$, $SrCeO_3$ and $LaNiO_3$/$SrCeO_3$ nanocomposite.

2.3. Characterizations technique

The crystallite size and type of the prepared nanomaterials was conducted by using the PANalytical diffractometer. The surface morphology was examined by FE-SEM (Mira3TESCAN). The absorbance properties and band gap of the prepared sample was recorded by UV-vis spectrophotometry (Agilent carry). The photoluminescence properties was recorded spectrophotometer (Shimadzu RF-5301). The chemical states of elements was recorded by X-ray photoelectron spectroscopy (XPS, VG ESCALab220i- XL). The electrochemical impedance (EIS) was studied by SP-240 Potentiostat.

2.4. Photocatalytic test

The photocatalysis test under UV light (450 W) was investigated using MB dye degradation at room temperature. MB degradation was studied in various exposure time intervals. The spectrophotometer is specifically developed for UV irradiation to analyze catalytic performance. The 30 mL of MB (10 mg/L) was used to this test. The distance of UV lamp from mixture was 13.3 cm. The equilibrium reaction was found after 30 min in dark condition. The $LaNiO_3$, $SrCeO_3$, and $LaNiO_3$/$SrCeO_3$ catalyst were used to this test. The reusability test was conducted by fifth cycle times. The photocatalysis mechanism was studied by using the scavenging test in the presence of silver nitrate, EDTA, vitamin C, and ethanol for quenching the e-, h+, $\bullet O_2^-$, and •OH.

2.5. Antibacterial test

The antimicrobial activity of the $LaNiO_3$/$SrCeO_3$ was determined by calculating the % inhibition of *Klebsiella pneumoniae* and *Bacillus cereus*. Here, the bacterial culture was inoculated and incubated at 37°C for 18 h. The culture was washed with saline water. The 5 mL of the nanosamples concentration (1, 15, 30, 60 mg) was added to 5 mL of bacterial cultures and shacked for 4 h. The OD of the solutions were recorded and the inhibition percentage was determined as the previous study [15].

2.6. Dopamine detection

The $LaNiO_3$/$SrCeO_3$ nanocomposites was applied as probe to

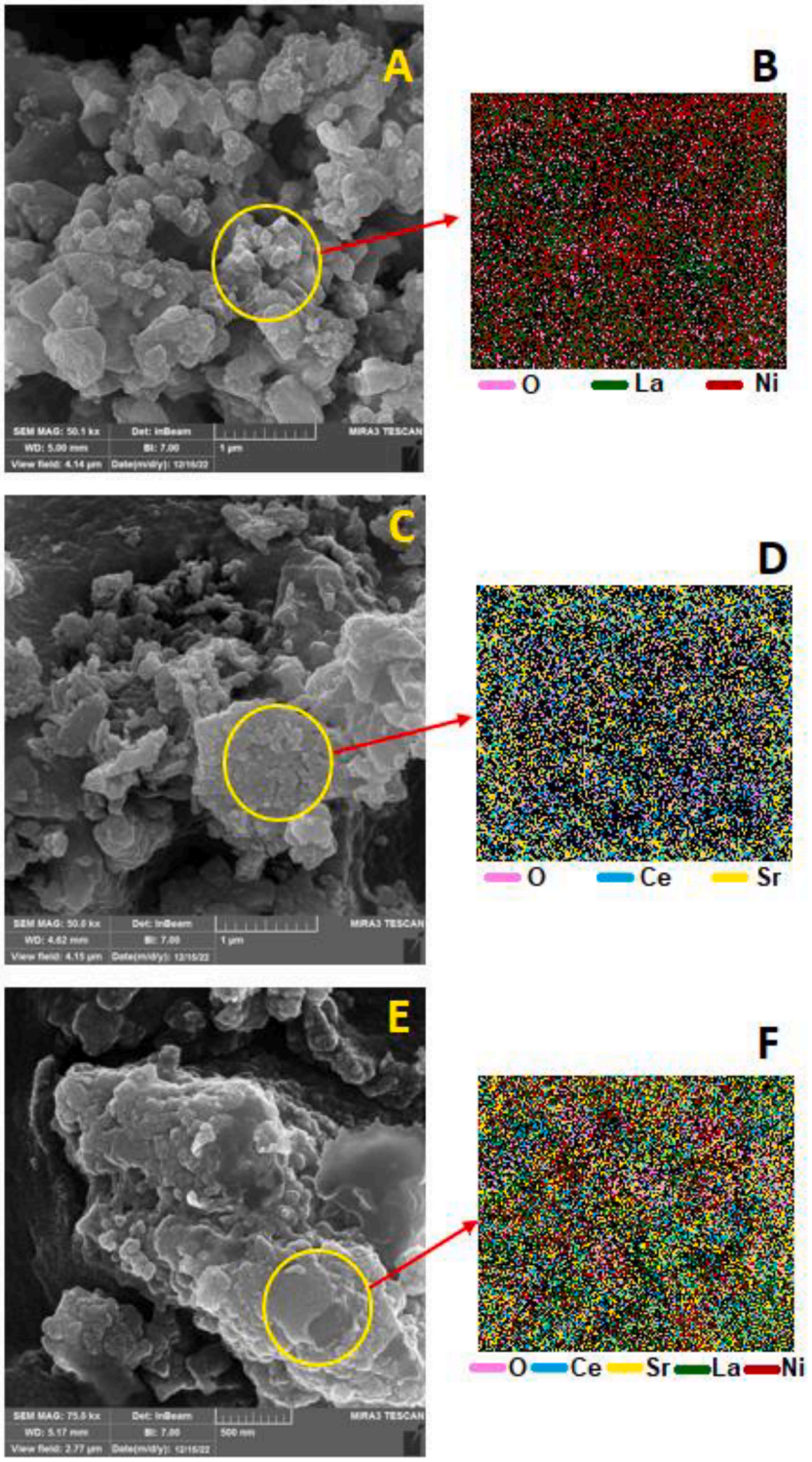

Fig. 2. FE-SEM and elemental mapping of (A, B) $LaNiO_3$, (C, D) $SrCeO_3$, (E, F) $LaNiO_3/SrCeO_3$ nanocomposite.

colorimetric detection of DA by using the H_2O_2/TMB in peroxidase activity. The interaction absorbance was spectrophotometrically monitored by using UV–visible (Agilent carry) spectroscopy. The reaction was conducted by the 50 μL of H_2O_2/TMB solution (1.0 mM to 1.0 mM), 5 mg/L of the $LaNiO_3/SrCeO_3$ were added to buffer solution. The selectivity of DA detection was studied by mixing the 30 μL of DA solutions and the interface compounds. The reaction was stirred at 40∘C for 30 min. The DA was detected from serum, and urine. The limit of detection for this method was calculated.

3. Results and discussion

3.1. Characterization

The X-ray (XRD) diffraction patterns of $LaNiO_3$, $SrCeO_3$, and $LaNiO_3/SrCeO_3$ nanocomposites are illustrated in Fig. 1. For $LaNiO_3$, the diffraction peaks relates with the planes (102), (110), (104), (202), (024), (116), (300), and (220) from hexagonal crystal structure (ICDD 79-2451) [26]. The diffraction peaks for $SrCeO_3$ are represented by the

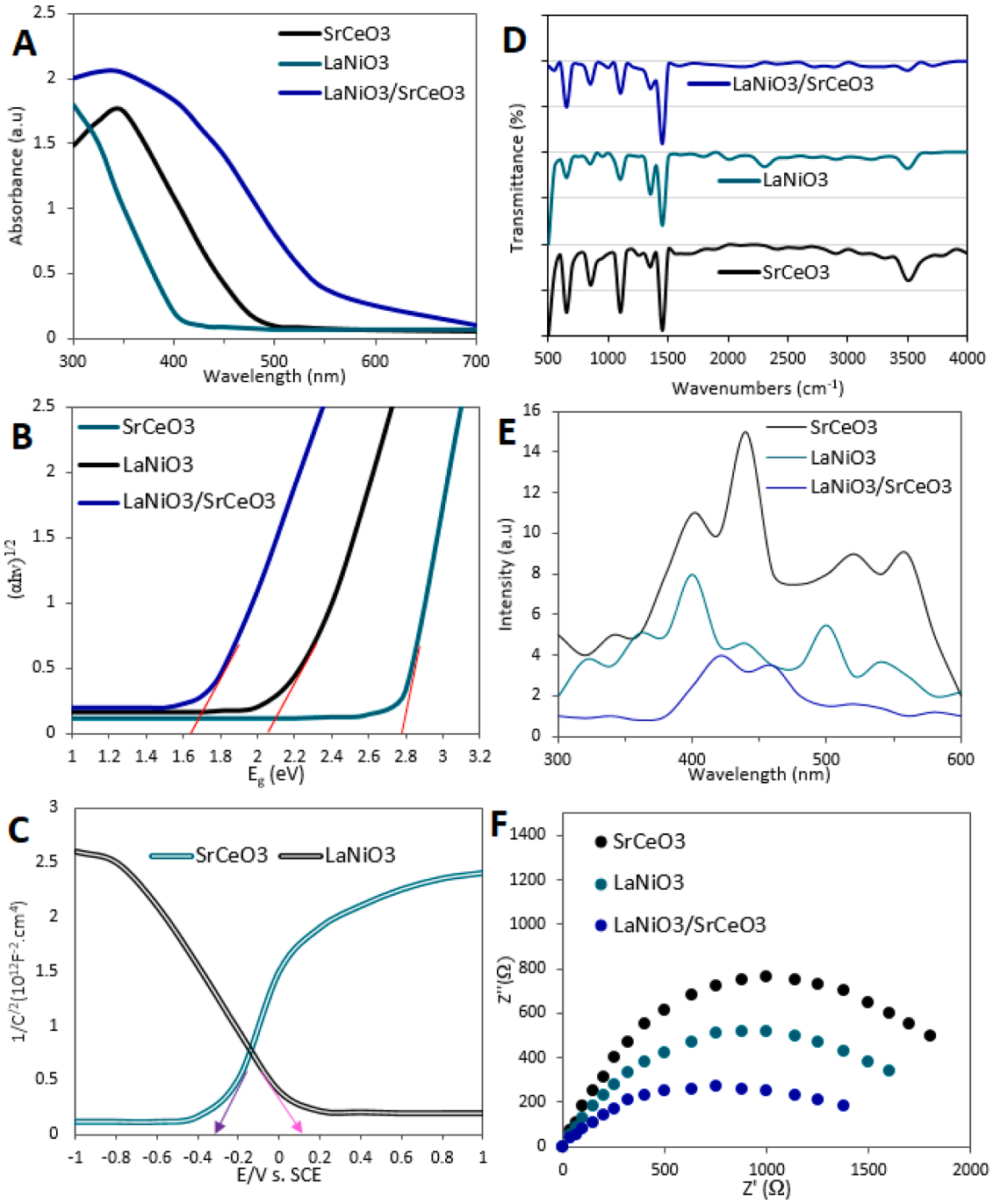

Fig. 3. (A) The absorbance vs wavelength, (B) energy band gap, (C) Mott-Schotty test, (D) FTIR spectra, (E) Photoluminescence spectra, and (F) EIS spectra for $LaNiO_3$, $SrCeO_3$ and $LaNiO_3/SrCeO_3$ nanocomposite

miller indices (020), (211), (311), (122), (411), (231), (213), and (520) from orthorhombic crystal (ICDD 81-26) [27]. The XRD curve of $LaNiO_3/SrCeO_3$ nanocomposites confirmed the presence of $LaNiO_3$, and $SrCeO_3$ nanoparticles in composite. The result shows that the crystalline phase of the $LaNiO_3/SrCeO_3$ nanocomposite without any impurities. Using the formula, the average crystallite size was estimated from the Debye–Scherer equation [15]. The average crystallite size of $LaNiO_3$, $SrCeO_3$, and $LaNiO_3/SrCeO_3$ nanocomposites is 18.3, 25.4, and 32.3 nm. Fig. 2 (A, B) depicts the FESEM images of $LaNiO_3$ nanoparticles with elemental mapping. It can be seen the spherical shape of $LaNiO_3$ nanoparticles with smooth surfaces. The elemental mapping shows the presence of La, Ni, and O. Fig. 2 (C, D) shows the irregular morphology of $SrCeO_3$ with the elemental mapping from Sr, Ce, and O. As shown in Fig. 2 (E, F), the surface morphology of the $LaNiO_3/SrCeO_3$ nanocomposite was spherical, with irregular shapes of agglomerated particles. As a result of the elemental mapping of the $LaNiO_3/SrCeO_3$ depicts the presence of La, Ni, Sr, Ce, and O in composites.

The optical properties of produced $LaNiO_3$, $SrCeO_3$, and $LaNiO_3/SrCeO_3$ materials were investigated UV-vis spectroscopy. The absorption measurements were performed to investigate the band gap level. The optical absorbance of $SrCeO_3$ was about 400 nm, and increase for $LaNiO_3$, and $LaNiO_3/SrCeO_3$ nanocomposites. The intensity of $LaNiO_3/SrCeO_3$ was higher than $SrCeO_3$, and $LaNiO_3$ in the UV region (Fig. 2A). Fig. 2B depicts the energy bandgap (Eg) from the Tauc relation expression [29–37]. As shown, the energy bandgap of $SrCeO_3$, $LaNiO_3$ and $LaNiO_3/SrCeO_3$ was found to be 2.79, 2.06, and 1.65 eV,

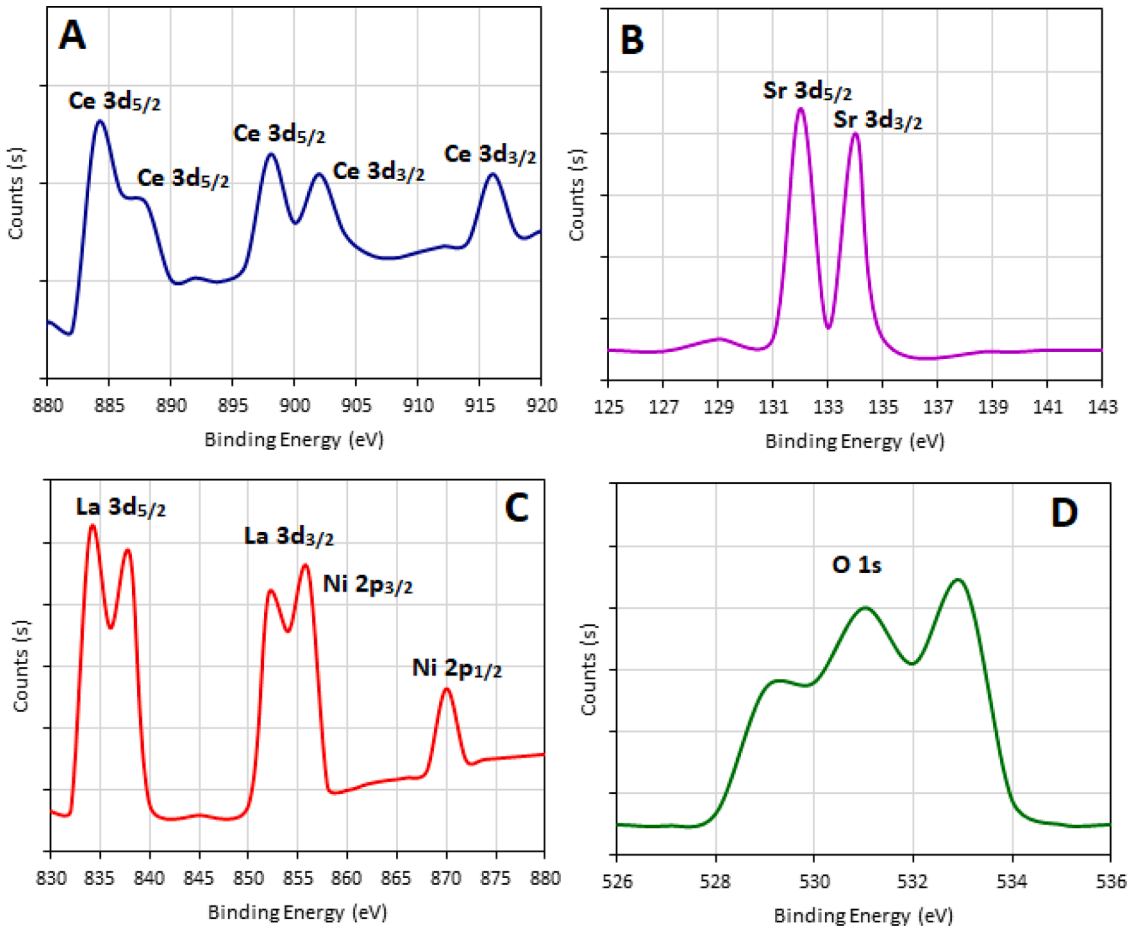

Fig. 4. XPS de-convoluted of (A) Ce 3d, (B) Sr 3d (C), La 3d, Ni 2p, and (D) O 1s from the $LaNiO_3/SrCeO_3$ nanocomposite.

respectively. The Mott-Schotty test was utilized to checking the flat band potential. As the previous studies, the p-type catalyst such as $LaNiO_3$, which that shows the activity in high wavelength compared to UV range via lower band gap. The n-type $SrCeO_3$ catalyst with wide band gap was activated in UV range [38–40]. The flat band potential of $LaNiO_3$ and $SrCeO_3$ was investigated and illustrated in the Fig. 2C. As can be observed that the positive slope of n-type $SrCeO_3$ and negative slope of p-type $LaNiO_3$ displayed the flat band potential properties [41–43]. Flat band potential values for $SrCeO_3$ and $LaNiO_3$ are -0.35 V and +0.13 V, respectively. FTIR spectra were used to examine the major functional groups existing in pure $LaNiO_3$, $SrCeO_3$, and $LaNiO_3/SrCeO_3$. Fig 3D displays $LaNiO_3$ with a weak absorption band at 3606 cm^{-1} in the IR region due to the presence of an O-H stretching vibration from water molecules [26]. Strong broad peaks around 637 cm^{-1} are related to metal-oxygen stretching vibrations. The sharp peak of about 1463 cm^{-1} and the weak peak of around 1384 cm^{-1} can be the asymmetric stretching of CO_3^{2-} functional groups. Furthermore, The C-H stretching is denoted by the peak at 1556.36 cm^{-1} and the C-O band is represented by the peaks at 1062 cm^{-1} and 854 cm^{-1}. As a result of FTIR spectra of $LaNiO_3/SrCeO_3$, indicating that the $SrCeO_3$ particles were coated with $LaNiO_3$ [27].

Photoluminescence (PL) and electrochemical impedance spectroscopy (EIS) were applied to investigate the rate of excitation of e^-/h^+ pair recombination for synthesized $LaNiO_3$, $SrCeO_3$, and $LaNiO_3/SrCeO_3$. PL measurement is the most effective method for studying the photo induced charge carrier properties of semiconductor materials. The photoluminescence of $LaNiO_3$, $SrCeO_3$, and $LaNiO_3/SrCeO_3$ were investigated. The $LaNiO_3$, $SrCeO_3$, and $LaNiO_3/SrCeO_3$ samples present substantial PL intensity signals and are represented in in Fig. 3E. The $SrCeO_3$ sample exhibited the highest intensity. As displayed, the $LaNiO_3/SrCeO_3$ nanocomposites has much lower PL intensity than the pure $LaNiO_3$ and $SrCeO_3$ samples, displaying that bonding with the $LaNiO_3$ layer on $SrCeO_3$ may minimize surface defects for charge recombination at an interface [48].

The electrochemical impedance spectroscopy (EIS) was studied to study charge transport carriers for the prepared samples. The EIS spectra were evaluated using the Nynquist plot was displayed in Fig. 3F. A lower arc radius, as is widely known, suggests less interference for electron-hole transmission, meaning that the performance has greater charge carrier separation [35]. The EIS result, demonstrates that the arc radius of the samples is ordered: $SrCeO_3$ > $LaNiO_3$ > and $LaNiO_3/SrCeO_3$ NC has the smallest arc radius, which indicates it has the lowest charge transfer impedance [47]. At low PL and EIS intensity exhibits that, fabricated hybrid $LaNiO_3/SrCeO_3$ has a lower recombination rate for induced photo-generated charge carriers, resulting the improved photocatalytic degradation efficiency [35]. XPS analysis was studied for information about the chemical and electronic state. XPS analysis of $LaNiO_3/SrCeO_3$ was conducted. Fig. 4 shows the high resolution XPS scan for the presence of lanthanum, nickel, strontium, cerium, and oxygen in composite. For Ce $3d_{5/2}$ and Ce $3d_{3/2}$ XPS spectrum (Fig. 4A), the de-convoluted peaks at 883.2, 889.4 and 897.9, 902.5 and 915.9 eV were suggested that the 4+ (IV) oxidation state of cerium in $SrCeO_3$ [27]. The Sr 3d spectrum (Fig. 4B) displays the two strongest peaks at 132.3 and 133.9 eV, which related to the Sr $3d_{5/2}$ and Sr $3d_{3/2}$ core-level spin-orbits of Sr^{2+} oxidation state, respectively [27]. The La 3d and Ni 2p XPS spectra was depicted in Fig. 4C. It can be seen that the La $3d_{3/2}$ peak overlap Ni $2p_{3/2}$ peak, and located at 855.4 eV [26]. The La $3d_{5/2}$ peak was observed at 834-837 eV. The Ni $2p_{1/2}$ peak was observed at 870.01 eV. The presence of La 3d and Ni 2p was observed, due to $LaNiO_3$ [26]. The O 1s can be de-convoluted into three binding energy peaks

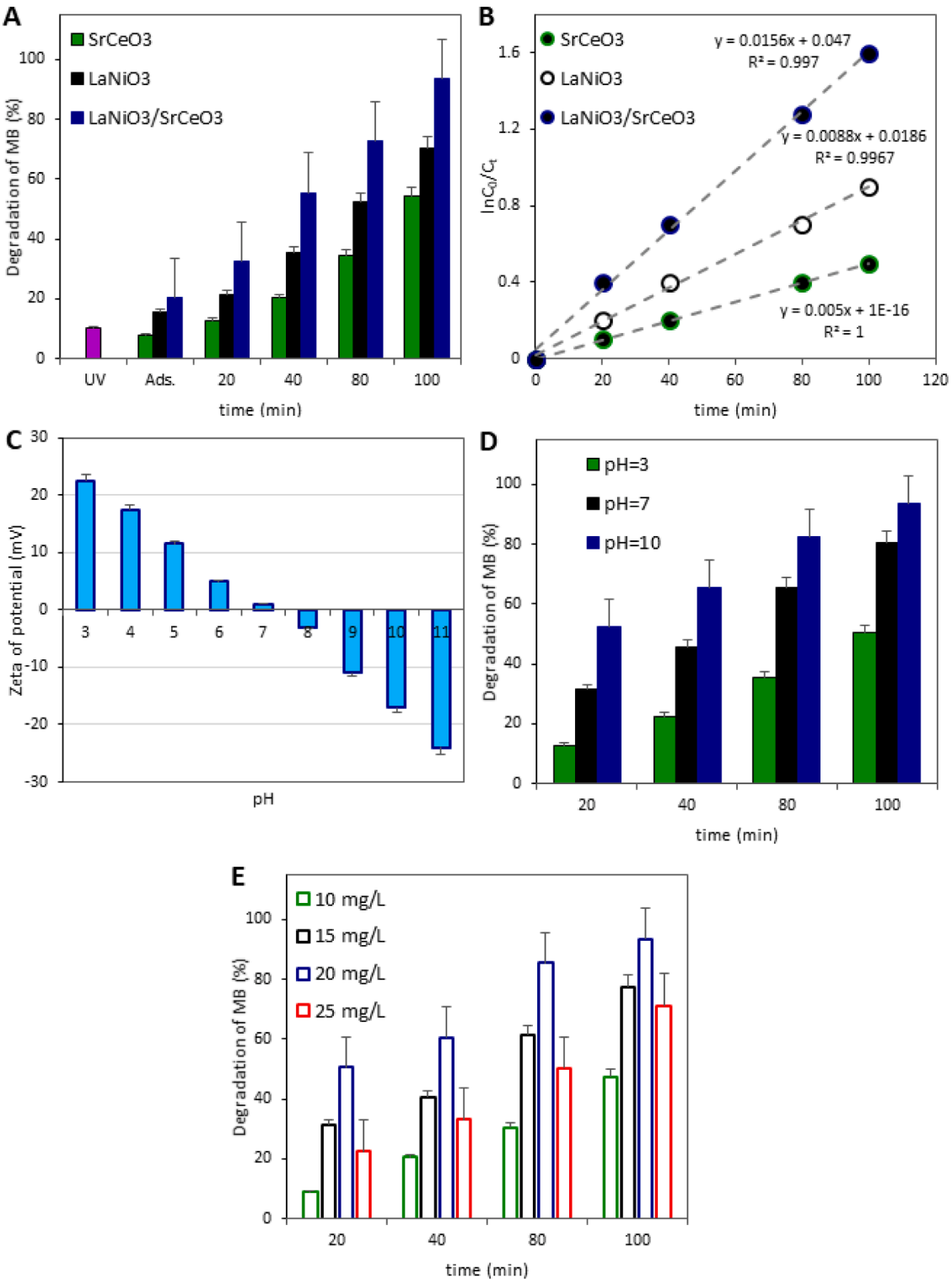

Fig. 5. (A) Degradation of MB dye for UV-light by different catalysts, (B) Photocatalytic reaction kinetics, (C) zeta potential of $LaNiO_3/SrCeO_3$ nanocomposite, (D) effect of pH on MB degradation, and (E) effect of catalyst dosage on MB degradation.

centered at 529.3, 531.5 and 532.8 eV were ascribed to the lattice oxygen, O-Sr, O-Ni, O-Ce, and O-La [26] (Fig. 4D).

3.2. Photocatalytic activity

The photocatalytic efficiency of the $LaNiO_3$, $SrCeO_3$, and $LaNiO_3/SrCeO_3$ nanocomposites were investigated by degradation of MB with UV irradiation. Fig. 5A shows the degradation of MB in different condition. It can be seen that the MB was degraded about 10% under UV light without any catalyst. The adsorption capacities of $LaNiO_3$, $SrCeO_3$, and $LaNiO_3/SrCeO_3$ were studied via removal of MB in dark condition. After 30 min, the adsorption capacities of $SrCeO_3$, $LaNiO_3$, and $LaNiO_3/SrCeO_3$ were found 8.31, 15.50, and 20.32%, respectively. The photocatalytic capacities of the prepared catalysts was investigated in different time (20-100 mins). As can be observed, the photocatalysis activity of $LaNiO_3/SrCeO_3$ was 93.50 % at 100 min, and it's higher than

Table 1
Comparison of photocatalytic degradation of MB.

Catalyst	Light source	Degradation	References
CeO2/SnO_2	UV	80 %	[54]
CeO_2/CuO	Visible	70 %	[55]
TiO_2/La_2O_3	UV	95 %	[56]
SnO_2/TiO_2	Visible	90 %	[57]
$LaNiO_3$/$SrCeO_3$	UV	93.5 %	This work

the activity of $SrCeO_3$ (54.35%), and $LaNiO_3$ (70.51%). The low band gap of $LaNiO_3$/$SrCeO_3$, and lower the PL intensity and arc radius can be present the substantial photocatalysis response for degradation of MB under UV light irradiation [44–53].

For different reaction times, Fig. 5B depicts the reaction kinetics of MB degradation by $SrCeO_3$, $LaNiO_3$, and $LaNiO_3$/$SrCeO_3$. The rate constant (K, min^{-1}) for photocatalytic degradation reactions for all catalysts was found from Fig. 5B. The rate constant (K, min^{-1}) of $SrCeO_3$, $LaNiO_3$, and $LaNiO_3$/$SrCeO_3$ was 0.0050, 0.0088, and 0.0156, respectively. It can be seen that the rate reaction of $LaNiO_3$/$SrCeO_3$ was 1.77, and 3.12 times higher than the $LaNiO_3$, and $SrCeO_3$ nanoparticles.

The pH is an important role in the photo-degradation of pollution. Fig.5C shows the effect of pH on degradation of MB under different times. Based on the results, the effectiveness of MB degradation under UV irradiation utilizing $LaNiO_3$/$SrCeO_3$ nanocomposite were 93.5% for alkaline media (pH=10), 80.51% for neutral media (pH=7), and 50.35% for acidic media (pH=3). The surface charges of $LaNiO_3$/$SrCeO_3$ at different pHs was investigated and displayed in Fig. 5D. The isoelectric point for $LaNiO_3$/$SrCeO_3$ is 7.0. The $LaNiO_3$/$SrCeO_3$ has negative charge at the higher isoelectric point. At acidic medium, the $LaNiO_3$/$SrCeO_3$ surface has positive charge, and reducing response due to the positive charge of the MB dye [54–56]. The stronger electrostatic interaction with MB and $LaNiO_3$/$SrCeO_3$ was done at basic medium. To evaluation of the catalyst dose effect on photocatalytic degradation, different dose of $LaNiO_3$/$SrCeO_3$ nanocomposites was added to the MB solution (Fig. 5E). The most effective catalyst dosage was 20 mg/L (93.5 %). The lower catalyst dose leads to less photon absorption by the $LaNiO_3$/$SrCeO_3$ nanocomposite, which results in decreasing the catalytic performance. At high catalyst concentrations (25 mg/L), the surface area of the catalyst decreases due to particle agglomeration [57].

Table 1 illustrates the comparison this study to a previous hybrid photocatalyst for the degradation of various organic pollutants. The synthesized $LaNiO_3$/$SrCeO_3$ nanocomposite displayed remarkable degradation efficiency for MB dye via exposed to UV–light. Catalyst regeneration in photocatalytic systems is a significant appearance of photocatalysis efficiency for the wastewater purification process [58–62]. After recycling the catalyst, the $LaNiO_3$/$SrCeO_3$ were applied for the degradation of fresh MB solution. This reaction was repeated for fifth cycle. Fig. 6A shows the recycling performance of catalytic efficiency. It can be seen that the photocatalysis capacity of the $LaNiO_3$/$SrCeO_3$ was negligibly decreased after 5^{th} cycle time (93.5% to 92.51%). The XRD of $LaNiO_3$/$SrCeO_3$ was studied after 5^{th} cycle time and are showed in Fig. 6B. The XRD analysis shows the stability of crystal phase after fifth photo-degradation reaction, and confirms the appreciable photostability of p-n type $LaNiO_3$/$SrCeO_3$ nanocomposite as a photocatalyst.

To determine the role of reactive species in the MB degradation, a scavenging analysis was conducted. Scavenging investigations paralleled the MB photo-degradation process. To detect such species, four scavengers, such as vitamin C (VC), ethanol (Et), Ethylene diamine tetra acetic acid (EDTA), and silver nitrate (SN) was added to the reaction to scavenging superoxide anions ($\bullet O_2^-$) radicals, hydroxyl radicals (•OH), holes (h^+), and electron (e^-), respectively (Fig. 6C). The presence of VC and Et reduces the MB decomposition (%). It can be seen that the presence of EDTA and SN can be decreased the photocatalysis amount, due to the •OH, and $\bullet O_2^-$ generated by using the h^+, and e^-, respectively, which that showed the •OH, and $\bullet O_2^-$ play important role in the MB degradation by $LaNiO_3$/$SrCeO_3$ nanocomposites [63–65].

The electron spin resonance (ESR) spectra was applied to evaluation of degradation mechanism as depicted in Fig. 6D, The high signals with intensities were observed for the DMPO–$\bullet O_2^-$ and DMPO–•OH under UV irradiation. The signal intensity of DMPO–•OH was approximately same to the DMPO–$\bullet O_2^-$, which that showed the •OH and $\bullet O_2^-$ are keys for MB degradation process by $LaNiO_3$/$SrCeO_3$ catalyst [66].

The diagrammatic mechanism for MB decomposition with $LaNiO_3$/$SrCeO_3$ nanocomposite is presented in Fig. 6E. The Mott-Schotty test shows the cunduction band of $SrCeO_3$ and $LaNiO_3$ are -0.35 V and +0.13 eV, respectively. The band gap of $SrCeO_3$ and $LaNiO_3$ was calculated from kubelka-munk plot, and are 2.79, and 2.06 eV, respectively. The valence band was calculated as below:

$$E_{VB} = E_{CB} + E_g \quad (1)$$

By using the equation, the valence band of $SrCeO_3$ and $LaNiO_3$ are 2.44, and 2.19 eV, respectively. When a $LaNiO_3$/$SrCeO_3$ semiconductor absorbs a photon, electron and hole were generated. Based on the energy diagram, the h^+ can be transferred from the VB of n-type $SrCeO_3$ to the VB of p-type $LaNiO_3$. The excited electrons can be transferred from the CB of p-type $LaNiO_3$ to the CB of n-type $SrCeO_3$. Thus, the p-n heterojunction $LaNiO_3$/$SrCeO_3$ has better photocatalytic response than the $LaNiO_3$ and $SrCeO_3$ [21]. Moreover, the VB potential of $LaNiO_3$ and $SrCeO_3$ are positive than the E_0= of •OH/H_2O (1.99 eV) [14], indicating that the h^+ on the surface of $LaNiO_3$ can be oxidize H_2O into •OH. In addition, the CB potential of $LaNiO_3$ is near to $SrCeO_3$ and are approximately negative to reduce the O_2 to the $\bullet O_2^-$ (E_0=-0.33 eV) [15]. Therefore, the role of •OH for degradation of MB was stronger than $\bullet O_2^-$ by using the p-n heterojunction $LaNiO_3$/$SrCeO_3$ nanocomposites under UV light irradiation, the presence of •OH and $\bullet O_2^-$ in system, can be MB degraded to CO_2 and H_2O.

3.3. Antibacterial activities

The antibacterial efficiecny of $SrCeO_3$, $LaNiO_3$ and $LaNiO_3$/$SrCeO_3$ was investigated against *Klebsiella pneumoniae* and *Bacillus cereus* and are reveled in Fig. S1. The antibacterial performance was investigated via various nano samples concentration. The inhibition percentage of nano samples on *K. pneumoniae* and *B. cereus* enhances with raise in the nano samples concentration. The inhibition percentage of $LaNiO_3$/$SrCeO_3$ was effective than $SrCeO_3$ and $LaNiO_3$ nanoparticles, due to the $LaNiO_3$/$SrCeO_3$ can be penetrates in the bacteria cell membrane, and inhibiting the formation of nucleic acid [67]. The production of ROS enhances the inhibition percentage of the nano $LaNiO_3$/$SrCeO_3$ material.

3.4. Colorimetric DA detection

In this work, the peroxidase like activity of the synthesized $LaNiO_3$/$SrCeO_3$ nanocomposites was investigated for detection of dopamine (DA) in the presence of TMB and H_2O_2. Fig. 7A depicts the absorbance spectra of different samples. It can be seen that the $LaNiO_3$/$SrCeO_3$ as probe without interaction with DA, has high absorbance in compared to other samples. The peroxidase activity of $LaNiO_3$/$SrCeO_3$ was great response in interaction with DA. It is noteworthy, the $LaNiO_3$/$SrCeO_3$ probe shows great response in interaction with DA in the presence of other compound such as urea, glutamic acid, arginine, valine, and lysine. Fig. 7B shows the effect of DA concentration on the peroxidase lick activity of the $LaNiO_3$/$SrCeO_3$ probe, which that showed the response of DA detection was enhanced in the lowest DA concentration. The LOD equation is [$Y = 0.2947\ X + 0.178$, $R^2 = 0.9868$], and calculated rom linear range of 1-200 nM [13–15]. The LOD was 3.48 nM (S/N = 10). The selectivity response of DA detection was studied by $LaNiO_3$/$SrCeO_3$ probe in the presence of other substance such as Urea, Glu A, Arg, Val, and Lys, and illustrated in Fig. 7C. The result depicts that the $LaNiO_3$/$SrCeO_3$ detect the DA via other compound without any

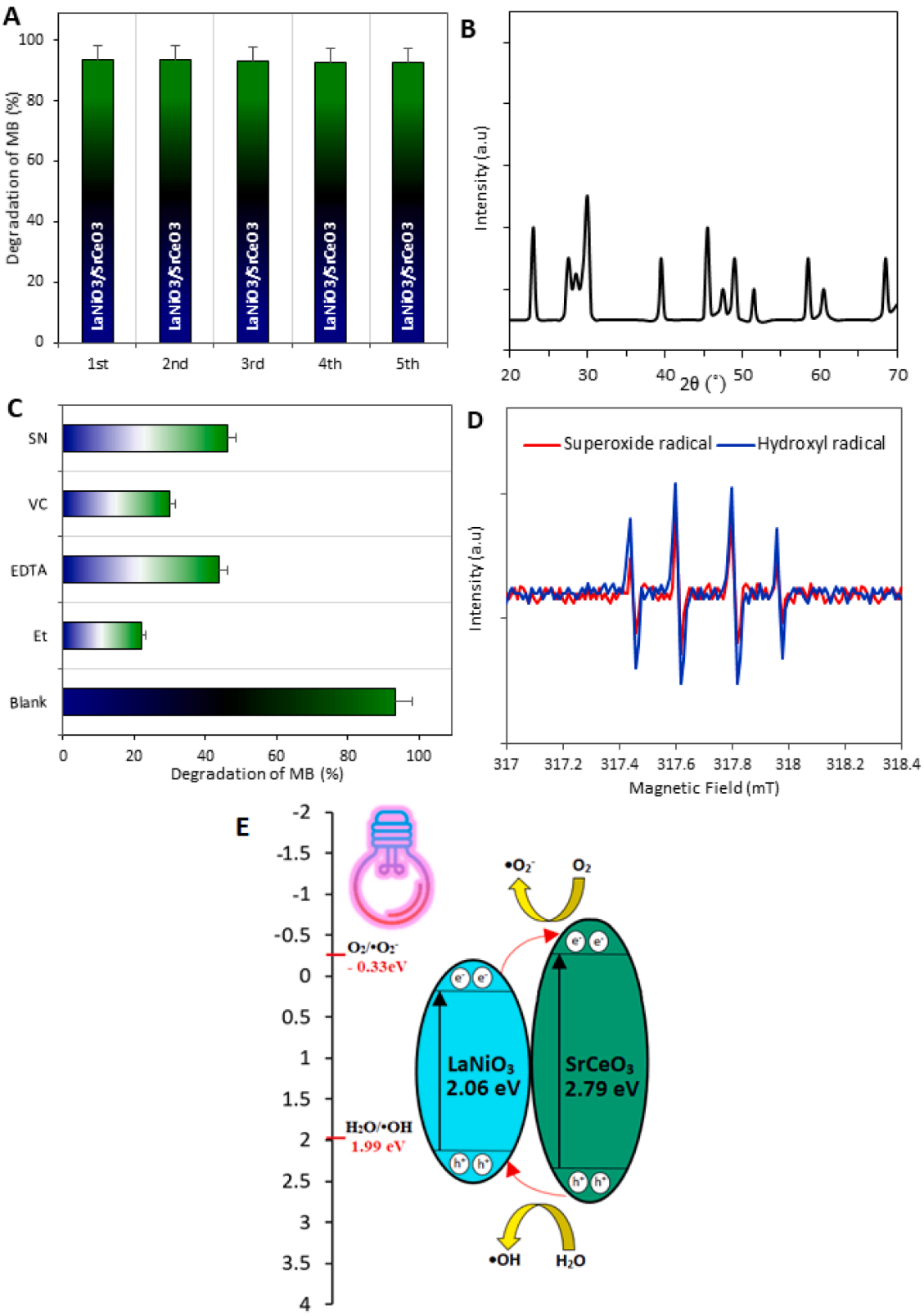

Fig. 6. (A) reusability test, (B) XRD of $LaNiO_3/SrCeO_3$ nanocomposite after 5th degradation of MB, (C) scavenging test, (D) DMPO spin-trapping ESR spectra of $LaNiO_3/SrCeO_3$, and (E) The possible photocatalytic mechanism.

noises. The accuracy of the prepared method was evaluated by the standard addition technique. After adding known concentration of DA (10, and 20 nM) into 1.0 mL of urine or serum, the probe was used to concentration of DA in two samples. Fig. 7D depicts the DA detection from urine and serum. It can be seen, DA detected as 9.8 and 19.9 nM in serum, and 10.2 and 21.2 nM in urine. The recovery rate of this probe is 98-106%.

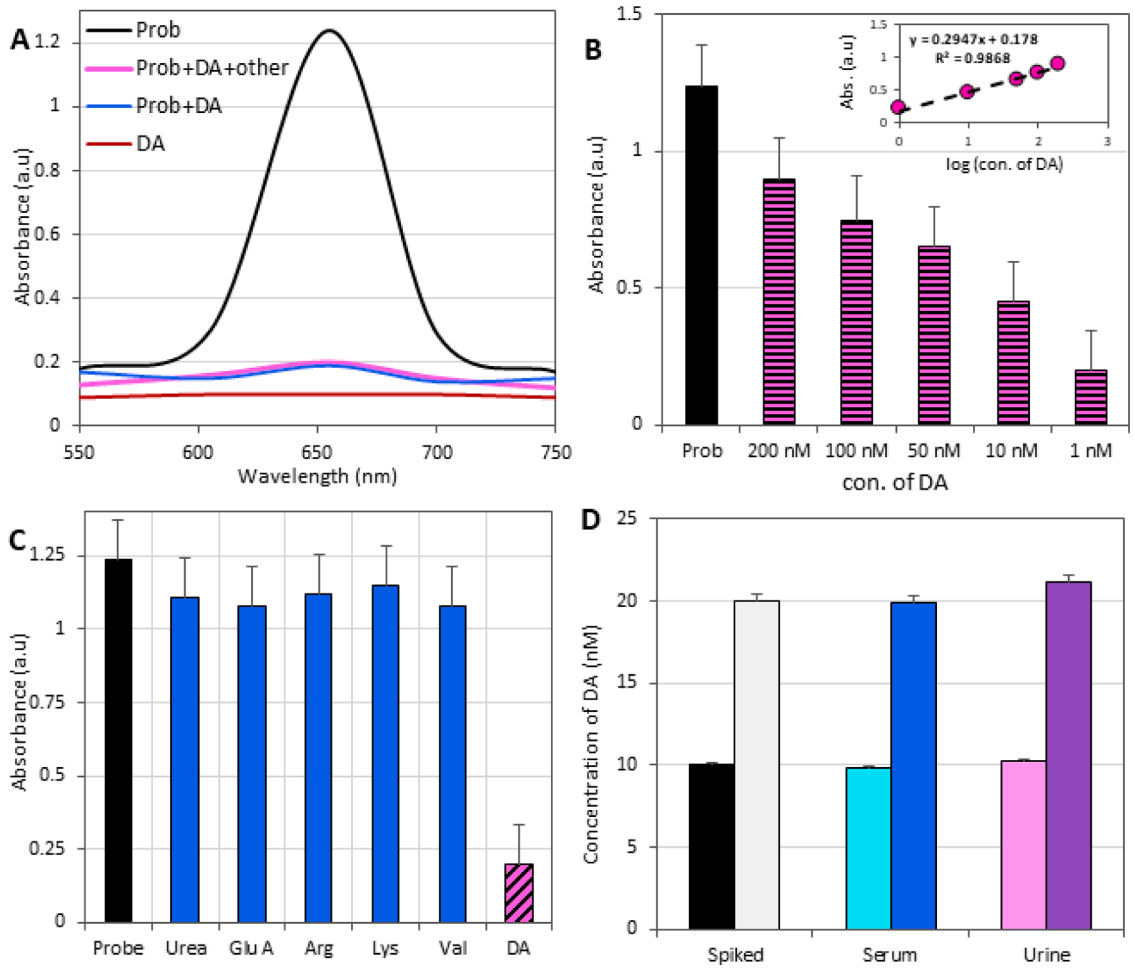

Fig. 7. (A) The peroxidase activity of samples in UV–vis spectra, (B) the effect of DA concentration (inset: calibration curve), (C) the selectivity DA detection, and (D) the DA detection from serum and urine.

4. Conclusion

In conclusion, a $LaNiO_3/SrCeO_3$ nanocomposites was prepared using a co-precipitation method, and the structural and optical properties were studied using various techniques. The XRD results the formation of a $LaNiO_3/SrCeO_3$ nanocomposites. The energy band gap of prepared nanocomposite was studied using UV-visible spectroscopy and shows that the combining of $LaNiO_3$ nanoparticles to $SrCeO_3$ can be decrease the energy band gap of $LaNiO_3/SrCeO_3$. The investigation confirms that the degradation of MB for LaNiO3/SrCeO3 nanocomposite was 93.5%, which is higher when compared to the pure LaNiO3 and SrCeO3 nanoparticles. The rate reaction of $LaNiO_3/SrCeO_3$ was 1.77, and 3.12 times higher than the $LaNiO_3$, and $SrCeO_3$ nanoparticles. Furthermore, the role of •OH for degradation of MB was stronger than $\bullet O_2^-$ by using the p-n heterojunction $LaNiO_3/SrCeO_3$ nanocomposites under UV light irradiation. The inhibition percentage of $LaNiO_3/SrCeO_3$ versus *Klebsiella pneumoniae* and *Bacillus cereus* was effective than $SrCeO_3$ and $LaNiO_3$ nanoparticles. The as-synthesized $LaNiO_3/SrCeO_3$ probe was used to dopamine detection. The probe depicts the superior analysis parameters. The LOD value of $LaNiO_3/SrCeO_3$ probe for DA detection was 3.48 nM.

CRediT authorship contribution statement

Ying Chen: Methodology, Investigation, Formal analysis. **Ali Jihad:** Formal analysis, Methodology, Investigation, Validation. **Fadhil Hussam:** Formal analysis, Methodology, Investigation. **Salah Hassan Zain Al-Abdeen:** Formal analysis, Methodology, Investigation. **Jamal Mohammad Hussein:** Formal analysis, Methodology, Investigation. **Zainab Hussein Adhab:** Formal analysis, Methodology, Investigation. **Zahraa Hamzaa Abd Alzahraa:** Formal analysis, Methodology, Investigation. **Irfan Ahmad:** Formal analysis, Methodology, Investigation, Validation, Resources. **Leila Fatolahi:** Investigation, Validation, Software, Data curation. **Baadal Jushi Janani:** Writing – review & editing, Methodology, Investigation, Validation, Software, Project administration, Conceptualization, Supervision.

Declaration of Competing Interest

The authors declare that they have no known competing financial interests or personal relationships that could have appeared to influence the work reported in this paper.

Data availability

The data that has been used is confidential.

Acknowledgement

The authors express their gratitude to the Deanship of Scientific Research at King Khalid University for funding this work through the Large Research Group Project under grant number RGP.02/316/44.

References

[1] FB. Elehinafe, O. Agboola, GO. Bamigboye, Insights on the advanced separation processes in water pollution analyses and wastewater treatment – a review, S. Afr. J. Chem. Eng. 42 (2022) 188–200.

[2] A. Mittal, R. Brajpuriya, R. Gupta, Solar steam generation using hybrid nanomaterials to address global environmental pollution and water shortage crisis, Mater. Today Sustainab. 21 (2023), 100319.

[3] Y. Wang, X. Cui, W. Lu, Synthesis of porphyrin porous organic polymers and their application of water pollution treatment: a review, Environ. Technol. Innovat. 29 (2023), 102972.

[4] A. Kausar, S.T. Zohra, A. Nazir, Cellulose-based materials and their adsorptive removal efficiency for dyes: a review, Int. J. Biol. Macromol. 224 (2023) 1337–1355.

[5] G.A. Ismail, H. Sakai, Review on effect of different type of dyes on advanced oxidation processes (AOPs) for textile color removal, Chemosphere 291 (2022), 132906.

[6] R. Tanveer, A. Yasar, Amtul Bari Tabinda, Integration of physical and advanced oxidation processes for treatment and reuse of textile dye-bath effluents with minimum area footprint, J. Cleaner Prod. 383 (2023), 135366.

[7] D.H.S. Santos, Ye Xiao, L. Meili, Regeneration of dye-saturated activated carbon through advanced oxidative processes: a review, Heliyon 8 (2022) e10205.

[8] Y. Yu, H. Huang, Coupled adsorption and photocatalysis of g-C3N4 based composites: material synthesis, mechanism, and environmental applications, Chem. Eng. J. 453 (2023), 139755.

[9] W. Long, M.U. Hamza, A. Fakhri, Preparation, photocatalytic and antibacterial studies on novel doped ferrite nanoparticles: characterization and mechanism evaluation, Colloids Surf. A 650 (2022), 129468.

[10] A. Bahadoran, N.B. Baghbadorani, A. Fakhri, Ag doped Sn_3O_4 nanostructure and immobilized on hyperbranched polypyrrole for visible light sensitized photocatalytic, antibacterial agent and microbial detection process, J. Photochem. Photobiol. B 228 (2022), 112393.

[11] Y.i. Mao, J. Qiu, A. Fakhri, A strategy of silver Ferrite/Bismuth ferrite nano-hybrids synthesis for synergetic white-light photocatalysis, antibacterial systems and peroxidase-like activity, J. Photochem. Photobiol. 426 (2022), 113756.

[12] Y. Liu, X.U. Zhou, V.K. Gupta, Evaluation of synergistic effect of polyglycine functionalized gold/iron doped silver iodide for colorimetric detection, photocatalysis, drug delivery and bactericidal applications, J. Photochem. Photobiol. 422 (2022), 113522.

[13] A. Bahadoran, Q. Liu, V.K. Gupta, Preparation of Sn/Fe nanoparticles for Cr (III) detection in presence of leucine, photocatalytic and antibacterial activities, Spectrochim. Acta Part A Mol. Biomol. Spectrosc. 253 (2021), 119592.

[14] X. Yao, Y.J. BahrAluloom, A. Fakhri, Multipurpose properties the Z-scheme dimanganese copper oxide/cadmium sulfide nanocomposites for photo- or photoelectro-catalytic, antibacterial applications, and thiamine detection process, J. Photochem. Photobiol. A 436 (2023), 114374.

[15] Z. Liu, M.A. Hadi, A. Fakhri, High efficiency of Ag0 decorated Cu_2MoO_4 nanoparticles for heterogeneous photocatalytic activation, bactericidal system, and detection of glucose from blood sample, J. Photochem. Photobiol. B 236 (2022), 112571.

[16] W. Bootluck, T. Chittrakarn, K. Techato, W. Khongnakorn, Modification of surface α-Fe2O3/TiO2 photocatalyst nanocomposite with enhanced photocatalytic activity by Ar gas plasma treatment for hydrogen evolution, J. Environ. Chem. Eng. 9 (2021), 105660.

[17] A. Fakhri, S. Behrouz, Comparison studies of adsorption properties of MgO nanoparticles and ZnO–MgO nanocomposites for linezolid antibiotic removal from aqueous solution using response surface methodology, Process Saf. Environ. Prot. 94 (2015) 37–43.

[18] A. Fakhri, S. Behrouz, V.K. Gupta, Synthesis and characterization of ZrO_2 and carbon-doped ZrO_2 nanoparticles for photocatalytic application, J. Mol. Liq. 216 (2016) 342–346.

[19] J. Sun†, X. Li, Q. Zhao, J. Ke, D. Zhang, Novel V_2O_5/$BiVO_4$/TiO_2 nanocomposites with high visible-light-induced photocatalytic activity for the degradation of toluene, J. Phys. Chem. 118 (2014) 10113–10121, 19.

[20] H. Lin, T. Li, A. Fakhri, Fabrication of Cu2MoS4 decorated WO_3 nano heterojunction embedded on chitosan: robust photocatalytic efficiency, antibacterial performance, and bacteria detection by peroxidase activity, J. Photochem. Photobiol. B 226 (2022), 112354.

[21] M. Zhang, N. Fang, X. Song, Y. Chu, S. Shu, Y. Liu, p–n heterojunction photocatalyst Mn0.5Cd0.5S/$CuCo_2S_4$ for highly efficient visible light-driven H_2 production, ACS Omega 5 (2020) 32715–32723, 50.

[22] S.M. Patil, A.G. Dhodamani, S.A. Vanalakar, et al., Multi-applicative tetragonal TiO_2/SnO_2 nanocomposites for photocatalysis and gas sensing, J. Phys. Chem. Solids 115 (2018) 127–136.

[23] S. Das, V.C. Srivastava, An overview of the synthesis of CuO-ZnO nanocomposite for environmental and other applications, Nanotechnol. Rev. 7 (2018) 267–282.

[24] S. Xiao, A. Fakhri, B.J. Janani, Synthesis of spinel Tin ferrite decorated on Bismuth ferrite nanostructures for synergetic photocatalytic, superior drug delivery, and antibacterial efficiencies, Surf. Interf. 27 (2021), 101490.

[25] M. Hosseini, A. Pourabadeh, A. Fakhri, J. Hallajzadeh, S. Tahami, Synthesis and characterization of Sb_2S_3-CeO_2/chitosan-starch as a heterojunction catalyst for photo-degradation of toxic herbicide compound: Optical, photo-reusable, antibacterial and antifungal performances, Int. J. Biol. Macromol. 118 (2018) 2108–2112.

[26] C. Chen, J. Zhou, J. Geng, R. Bao, Z. Wang, J. Xia, H. Li, Perovskite $LaNiO_3$/TiO_2 step-scheme heterojunction with enhanced photocatalytic activity, Appl. Surf. Sci. 503 (2020), 144287.

[27] P. Sundaresan, R. Karthik, S.-M. Chen, J. Vinoth Kumar, V. Muthuraj, E. R. Nagarajan, Ultrasonication-assisted synthesis of sphere-like strontium cerate nanoparticles (SrCeO3 NPs) for the selective electrochemical detection of calcium channel antagonists nifedipine, Ultrason. Sonochem. 53 (2019) 44–54.

[28] D.S. Kim, E.S. Kang, S. Baek, S.S. Choo, Y.H. Chung, D. Lee, M. Junhong, T. Hyung Kim, Electrochemical detection of dopamine using periodic cylindrical gold nanoelectrode arrays, Sci. Rep. 8 (2018) 14049.

[29] J. Wang, Z. Wang, J. Zhang, S.-P. Chai, K. Dai, J. Low, Surface-active site modulation of the S-scheme heterojunction toward exceptional photocatalytic performance, Nanoscale 14 (2022) 18087–18093.

[30] X. Li, J. Zhang, Y. Huo, K. Dai, S. Li, S. Chen, Two dimensional sulfur- and chlorine-codoped g-C_3N_4/CdSe-amine heterostructures nanocomposite with effective interfacial charge transfer and mechanism insight, Appl. Catal. B 280 (2021), 119452.

[31] K. Dai, J. Lv, J. Zhang, G. Zhu, L. Geng, C. Liang, Efficient visible-light-driven splitting of water into hydrogen over surface-fluorinated anatase TiO_2 nanosheets with exposed {001} facets/layered CdS–diethylenetriamine nanobelts, ACS Sustain Chem. Eng. 6 (2018) 12817–12826.

[32] T. Hu, K. Dai, J. Zhang, S. Chen, Noble-metal-free Ni2P modified step-scheme SnNb2O6/CdS-diethylenetriamine for photocatalytic hydrogen production under broadband light irradiation, Appl. Catal. B 269 (2020), 118844.

[33] Yang, H., feng Zhang, J., Dai, K. Organic amine surface modified one-dimensional CdSe0.8S0.2-diethylenetriamine/two-dimensional SnNb2O6 S-scheme heterojunction with promoted visible-light-driven photocatalytic CO2 reduction, 43, 2022, 255–264.

[34] X. Li, Z. Wang, J. Zhang, K. Dai, K. Fan, G. Dawson, Branch-like CdxZn1-xSe/Cu2O@Cu step-scheme heterojunction for CO2 photoreduction, Mater. Today Phys. 26 (2022), 100729.

[35] X. Ke, J. Zhang, K. Dai, Ke Fan, C. Liang, Integrated S-scheme heterojunction of amine-functionalized 1D CdSe nanorods anchoring on ultrathin 2D $SnNb_2O_6$ nanosheets for robust solar-driven CO_2 conversion, Sol. RRL 5 (2021), 2000805.

[36] L. Liu, T. Hu, K. Dai, J. Zhang, C. Liang, A novel stepscheme $BiVO_4$/Ag_3VO_4 photocatalyst for enhanced photocatalytic degradation activity under visible light irradiation, Chin. J. Catal. 42 (2021) 46–55.

[37] T. Hu, K. Dai, J. Zhang, G. Zhu, C. Liang, One-pot synthesis of step-scheme Bi2S3/porous g-C3N4 heterostructure for enhanced photocatalytic performance, Mater. Lett. 257 (2019), 126740.

[38] Y. Liu, Y.C. Zhang, X.F. Xu, Hydrothermal synthesis and photocatalytic activity of CdO2 nanocrystals, J. Hazard Mater 163 (2009) 1310–1314.

[39] T. Ge, Z. Jiang, L. Shen, J. Li, Z. Lu, Y. Zhang, F. Wang, Synthesis and application of Fe_3O_4/$FeWO_4$ composite as an efficient and magnetically recoverable visible light-driven photocatalyst for the reduction of Cr(VI), Sep. Purif. Technol. 263 (2021), 118401.

[40] T. Ge, L. Shen, J. Li, Y. Zhang, Y. Zhang, Morphology-controlled hydrothermal synthesis and photocatalytic Cr(VI) reduction properties of α-Fe_2O_3, Colloids Surf. A 635 (2022), 128069.

[41] J. Li, T. Peng, Y. Zhang, C. Zhou, A. Zhu, Polyaniline modified SnO_2 nanoparticles for efficient photocatalytic reduction of aqueous Cr(VI) under visible light, Sep. Purif. Technol. 201 (2018) 120–129.

[42] F. Zhang, Y. Zhang, Y. Zhang, Efficient photocatalytic reduction of aqueous Cr (VI) by Zr4+ doped and polyaniline coupled SnS_2 nanoflakes, Sep. Purif. Technol. 283 (2022), 120161.

[43] H. Wei, Y. Zhang, Y. Zhang, Y. Zhang, Design and synthesis of a new highefficiency CeO2/SnS2/polyaniline ternary composite visible-light photocatalyst, Colloid Interface Sci. Commun. 45 (2021), 100550.

[44] M. Zhou, T. Tang, D. Qin, H. Cheng, X. Wang, J. Chen, G. Hu, Hematite nanoparticle decorated MIL-100 for the highly selective and sensitive electrochemical detection of trace-level paraquat in milk and honey, Sens. Actuators B 376 (2023), 132931, https://doi.org/10.1016/j.snb.2022.132931.

[45] Z. Wu, C. Li, F. Zhang, S. Huang, F. Wang, X. Wang, H. Jiao, High-performance ultra-narrow-band green-emitting phosphor LaMgAl11O19:Mn2+ for wide color-gamut WLED backlight displays, J. Mater. Chem. C 10 (19) (2022) 7443–7448, https://doi.org/10.1039/D2TC00850E.

[46] Z. Huang, J. Ding, X. Yang, H. Liu, P. Song, Y. Guo, W. Zhan, Highly efficient oxidation of propane at low temperature over a Pt-based catalyst by optimization support, Environ. Sci. Technol. 56 (23) (2022) 17278–17287, https://doi.org/10.1021/acs.est.2c05599.

[47] N. Zhang, Y. Guo, Y. Guo, Q. Dai, L. Wang, S. Dai, W. Zhan, Synchronously constructing the optimal redox-acidity of sulfate and RuO_x Co-modified CeO_2 for catalytic combustion of chlorinated VOCs, Chem. Eng. J. 454 (2023), 140391, https://doi.org/10.1016/j.cej.2022.140391.

[48] P. Xu, C. Ding, Z. Li, R. Yu, H. Cui, S. Gao, Photocatalytic degradation of air pollutant by modified nano titanium oxide (TiO2) in a fluidized bed photoreactor: Optimizing and kinetic modeling, Chemosphere 319 (2023), 137995, https://doi.org/10.1016/j.chemosphere.2023.137995.

[49] K. Yang, Q. Geng, Y. Luo, R. Xie, T. Sun, Z. Wang, J. Tian, Dysfunction of FadA-cAMP signalling decreases Aspergillus flavus resistance to antimicrobial natural preservative Perillaldehyde and AFB1 biosynthesis, Environ. Microbiol. 24 (3) (2022) 1590–1607, https://doi.org/10.1111/1462-2920.15940.

[50] R. Yang, E. Hou, W. Cheng, X. Yan, T. Zhang, S. Li, Y. Guo, Membrane-targeting neolignan-antimicrobial peptide mimic conjugates to combat methicillin-resistant staphylococcus aureus (MRSA) infections, J. Med. Chem. 65 (2022) 16879–16892, https://doi.org/10.1021/acs.jmedchem.2c01674, 24.

[51] K. Zhang, Q. Deng, J. Luo, C. Gong, Z. Chen, W. Zhong, H. Wang, Multifunctional Ag(I)/CAAA-amidphos complex-catalyzed asymmetric [3+2] cycloaddition of α-substituted acrylamides, ACS Catal. 11 (9) (2021) 5100–5107, https://doi.org/10.1021/acscatal.1c00913.
[52] W. Guo, H. Luo, Z. Jiang, D. Fang, J. Chi, W. Shangguan, A.F. Lee, Ge-doped cobalt oxide for electrocatalytic and photocatalytic water splitting, ACS Catal. 12 (19) (2022) 12000–12013, https://doi.org/10.1021/acscatal.2c03730.
[53] F. Hu, L. Qiu, W. Xia, C. Liu, X. Xi, S. Zhao, N. Su, Spatiotemporal evolution of online attention to vaccines since 2011: an empirical study in China, Front Public Health (2022), https://doi.org/10.3389/fpubh.2022.949482.
[54] E. Kusmierek, A CeO_2 semiconductor as a photocatalytic and photoelectrocatalytic material for the remediation of pollutants in industrial wastewater: a review, Catalysts 10 (2020) 1–54, https://doi.org/10.3390/catal10121435.
[55] R. Saravanan, S. Joicy, V.K. Gupta, Visible light induced degradation of methylene blue using CeO_2/V_2O_5 and CeO_2/CuO catalysts, Mater Sci. Eng. C 33 (2013) 4725–4731.
[56] S. Sudhagar, S.S. Kumar, I.J.I. Premkumar, UV- and visible-light-driven TiO_2/La_2O_3 and TiO_2/Al_2O_3 nanocatalysts: synthesis and enhanced photocatalytic activity, Appl Phys A Mater Sci Process 128 (2022) 282.
[57] S. Kavitha, N. Jayamani, D. Barathi, Investigation on SnO_2/TiO_2 nanocomposites and their enhanced photocatalytic properties for the degradation of methylene blue under solar light irradiation, Bull Mater Sci. 44 (2021) 26.
[58] V. Andalib, J. Sarkar, A system with two spare units, two repair facilities, and two types of repairers, Mathematics 10 (6) (2022) 852, https://doi.org/10.3390/math10060852.
[59] T. Alizadeh, R. Jahani, A new strategy for low temperature gas sensing by nano-sized metal oxides: development a new nerve agent simulant sensor, Mater. Chem. Phys. 168 (2015) 180–186, https://doi.org/10.1016/j.matchemphys.2015.11.019.
[60] M. Yosofvand, S. Liyanage, N.S. Kalupahana, S. Scoggin, N. Moustaid-Moussa, H. Moussa, AdipoGauge software for analysis of biological microscopic images, Adipocyte 9 (1) (2020) 360–373, https://doi.org/10.1080/21623945.2020.1787583.
[61] A. Zakaria, S.A.I. Asaduzzaman, Z. Nahar, H.J. Snigdha, T. Murshed, R. Noor, A short review of the genes involved in the development and progression of colorectal cancer, Biocell 45 (3) (2021) 483, https://doi.org/10.32604/biocell.2021.014704.
[62] R.M. Nejad, N. Sina, W. Ma, Z. Liu, F. Berto, A. Gholami, Optimization of fatigue life of pearlitic Grade 900A steel based on the combination of genetic algorithm and artificial neural network, Int. J. Fatigue 162 (2022), 106975, https://doi.org/10.1016/j.ijfatigue.2022.106975.
[63] S.A. Hashemi, K. Farhangdoost, W. Ma, D.G. Moghadam, R.M. Nejad, F. Berto, Effects of tensile overload on fatigue crack growth in AM60 magnesium alloys, Theor. Appl. Fract. Mech. 122 (2022), 103573, https://doi.org/10.1016/j.tafmec.2022.103573.
[64] L. Berry, G. Wheatley, W. Ma, R.M. Nejad, F. Berto, The influence of milling induced residual stress on fatigue life of aluminum alloys, Forces Mech. 7 (2022), 100096, https://doi.org/10.1016/j.finmec.2022.100096.
[65] F. Peng, X. Xie, K. Wu, Y. Zhao, L. Ren, Online hierarchical energy management strategy for fuel cell based heavy-duty hybrid power systems aiming at collaborative performance enhancement, Energy Convers. Manage. 276 (2023), 116501, https://doi.org/10.1016/j.enconman.2022.116501.
[66] X. Cao, Q. Luo, F. Song, G. Liu, S. Chen, Y. Li, Y. Lu, Effects of oxidative torrefaction on the physicochemical properties and pyrolysis products of hemicellulose in bamboo processing residues, Ind. Crops Prod. 191 (2023), 115986, https://doi.org/10.1016/j.indcrop.2022.115986.
[67] Y. Lu, Q. Luo, X. Jia, J.P. Tam, H. Yang, Y. Shen, X. Li, Multidisciplinary strategies to enhance therapeutic effects of flavonoids from Epimedii Folium: Integration of herbal medicine, enzyme engineering, and nanotechnology, J. Pharm. Anal. (2022), https://doi.org/10.1016/j.jpha.2022.12.001.